Learning Spectral Calibration Parameters For Color Inspection

P. Carvalho, A. Santos, A. Dourado, B. Ribeiro
Centre for Informatics and Systems, Informatics Eng. Dep., University of Coimbra
Pólo II, Pinhal de Marrocos, 3030 Coimbra, Portugal
Email: {carvalho, amancio, dourado, bribeiro}@dei.uc.pt

Abstract

Light sensor spectral calibration is an ill-defined problem. For the identification problem one needs a priori knowledge of the characteristics of the sensor, which is difficult to get in most situations. A new methodology is presented in this paper that does not rely on any a priori knowledge of the sensor's characteristics. The method uses an extended generalized cross-validation function to measure predictability of the identified sensor's spectral behavior. The prediction error is minimized with a hybrid genetic algorithm. Further, an extended image formation model is introduced to model changes in additive and multiplicative errors. The calibration problem is formulated to be independent of these changes by previously identifying and removing them from the images.

1. Introduction

There are several situations in color vision (namely in physics-based), such as illumination and reflectance estimation [8], color correction [5], demosaicing [19], just to name a few, where the knowledge of the sensor's spectral sensitivities is desirable, if not fundamental. The computation of these sensitivities usually requires the sensor to be exposed to luminous signals with known SPDs (Spectral Power Distribution). The intended input-output relations are obtained indirectly with error minimization techniques, or directly through sampling. Indirect sensitivity estimation is an ill-posed problem due to its integral nature, i. e., the sensor's sensitivity does not depend continuously on its output, since there are rapidly oscillating functions which come arbitrarily close to being annihilated by the integral operator. On the other hand, natural colors can be reasonably well approximated with just a few basis functions which drastically reduces the number of linear independent constraints for identification. Therefore, it is seen that most methods impose some smoothness constraints to promote realistic estimations. In Lee's [13] calibration method a Macbeth-ColorChecker color map is applied,which is composed by 24 distinct color and gray scale patches. Using the 24 patches and assuming the knowledge of the illumination's SPD, an under-constrained linear equation set is obtained. It turns out that the solution is very noise dependant. Sharma and Trussel [17] introduced some additional constraints to force causal and smooth estimations. Basically, they impose an upper limit on the function's roughness. It can be proven [7] that this approach is equivalent to a Butterworth low-pass filter, being the cut-off frequency controlled by the roughness threshold. Barnard and Funt [1] linearized these constraints and formulated the calibration problem to enable a least squares with linear constraints solution. Given the importance of the smoothness constraint for the calibration task, several approaches have been introduced. Hubel et al. [12] used a Wiener filter to improve and enable smooth estimations. They model the covariance matrix as a first order Markov process where smoothness is imposed by a user specified correlation coefficient between adjacent elements. Finlayson and Hordly [9] tackled the problem by limiting the frequency components of the sensitivity function $S(\lambda)$ through modeling with Fourier's 9 to 15 first basis functions. In [9] further constraints are formulated on the solution's modality. The above approaches on indirect estimation techniques require precise *a priori* knowledge of the sensitivity curves to be computed to formulate hard constraints for the identification problem. A different approach is described in [19], enabling direct spectral sensitivity functions' sampling. Although very promising, the method implies the use of a monochromator to generate known and narrowband luminous signals which are then applied directly to the light sensor.

Automatic color inspection is a special case of color vision since usually it may be assumed that the illumination source and the lens are a property of the system. Hence, it suffices to calibrate $Q(\lambda) \equiv I_E(\lambda)S(\lambda)L(\lambda)$, being $L(\lambda)$ the spectral distortion introduced by the lens and $I_E(\lambda)$ the SPD of the illumination source. Recently we have introduced a method to estimate $Q(\lambda)$ based on calibrated color reference charts [2]. In our method, smoothness is

promoted with a regularization term based on the second derivative of $Q(\lambda)$. We observed [2] that an increase in the approximation error, for large regularization gains, is mainly due to excessive attenuation introduced in local maxima, for large changes in slope occur. We derived a new method [3] based on maxima estimation and constraining that is able to stabilize the estimation error. As all mentioned indirect and direct estimation techniques, it assumes that (i) the noise sources in image formation are stable over time (for real cameras this is usually not verified), (ii) some *a priori* knowledge is available on the function's shape (although in our method this is a mild condition) and (iii) maxima are precisely estimated (for band-limited function in the red region, usually some errors are committed).

In this paper a new method is introduced for spectral camera calibration which is able to learn the needed knowledge from the input data. The method uses an extended generalized cross-validation function GCV_{IC} to measure the prediction ability of the estimated function. The prediction ability is then maximized using a combined genetic algorithm (GA) with a golden section line search technique. In this method an image formation model is applied, where variability of multiplicative and additive errors are assumed. These errors are accounted for by the algorithm.

2. Image formation model

Noise is an intrinsic property of the image formation process. Healey and Kondepudy [11] have identified the main noise sources which occur in the image formation process and have described a set of algorithms for their correction and characterization. In their method, it is assumed that the noise characteristics are static over time, i. e., their means and variances do not vary. In practice, this behavior is only verified under very restricted conditions. For instance, the model assumes that dark current noise is stable. However, given its high temperature dependance, this assumption will only be verified if the temperature of the image acquisition environment is kept constant. Further, the model assumes that the overall gain of each image formation channel does not vary from image to image. Several authors [18][5] have pointed out variations in channel gain. Hence we use the following extension to Healey's and Kondepudy's image formation model. Let $\xi(u,v,t)$ be the linearized camera output for point (u,v) at instant t, then

$$\xi(u,v,t) = \mu_\xi(u,v,t) + N(u,v,t) \tag{1}$$

where $N(u,v,t)$ is a random variable of mean 0 and variance $\sigma_N^2(u,v,t)$ induced by shot, read and quantization noise and μ_ξ defined as in (2).

$$\begin{aligned}\mu_\xi(u,v,t) = A(t)\{S_R(u,v)\,I(u,v,t) + \\ N_D(u,v,\tau(t)) + N_o(u,v)\} + \mu_F(u,v,t)\end{aligned} \tag{2}$$

In (2) $A(t)$, $S_R(u,v)$, $N_D(u,v,\tau(t))$, $\tau(t)$, $N_o(u,v)$ and $\mu_F(u,v,t)$ represent, respectively, the channel gain, the fixed pattern noise in charge collection, the dark current charge, the temperature, other background charge such as fat zero and internal luminance ($N_o(u,v) \ll N_D(u,v,\tau(t))$ and $N_o(u,v) \approx constant$ spatially and over time) and the offset introduced by the camera's transfer function for pixel (u,v). $I(u,v,t)$ is defined as $\int_{\lambda_0}^{\lambda_n} I(\lambda,u,v,t)\,S(\lambda)\,d\lambda$, being $I(\lambda,u,v,t)$ the SPD of the input radiation at point (u,v) for instant t. For cameras with almost linear transfer functions (note that, even for so called linear cameras, the transfer function may not exhibit linearity due to charge collection sites capacitance dependence on collected charge [16]), it can be shown that $\mu_F(u,v,t) \to 0$ and σ_N^2 is a linear function of $\mu_\xi(u,v,t)$.

Dark current is generated by thermal electron excitation. According to [10] the number of collected electrons at each collection site due to temperature effects follows a Boltzmann distribution. Real solid state sensors exhibit dark current noise variations from site to site, which is mainly due to the inability of producing exact alike sensor cells. Hence, we characterize the dark current noise to be

$$N_D(u,v,\tau(t)) = K_D(u,v)\,\eta(\tau(t)) \tag{3}$$

where $K_D(u,v)$ is a random variable with mean 1 and spacial variance $\sigma_{N_D}^2$.

Let $R(\lambda,t)$ be the reflectance of a dielectric, non homogeneous and planar surface at instant t, and let $I_E(\lambda)$ be the SPD of an artificial incandescent light source projected on that surface. From the dichromatic reflection model, if a convenient geometrical setup is chosen, then it is seen that the light reflected from these surfaces can be modeled by the body reflection component [2], i. e., $I(\lambda,u,v,t) = C_I(u,v) I_E(\lambda) R(\lambda,t)$, where $C_I(u,v) \in [0,1]$ accounts for the geometrical dependent light power distribution and reflection attenuation. Before light interacts with a sensor's cell it has to travel through the lens system which introduces further attenuation and spectral transformation. Let $L(\lambda)$ be the spectral transmittance of the lens system and $C_L(u,v)$ be its light attenuation effect (such as the $\cos^4$ and the vignetting effects), then

$$I(\lambda,u,v,t) = C_I(u,v) C_L(u,v) I_E(\lambda) R(\lambda,t) L(\lambda) \tag{4}$$

Hence, combining (1), (3) and (4), and assuming that the camera's transfer function is reasonably linear, it follows that each linearized pixel output may be described by

$$\begin{aligned}\xi(u,v,t) \;=\; & C(u,v)A(t) \times \\ & \times \int_{\lambda_0}^{\lambda_n} Q(\lambda)\,R(\lambda,t)\,d\lambda + A(t)N_o(u,v) \\ & + A(t)K_D(u,v)\,\eta(\tau(t)) + N(u,v,t)\end{aligned} \tag{5}$$

where $Q(\lambda) \equiv I_E(\lambda) L(\lambda) S(\lambda)$ and $C(u,v) \equiv C_I(u,v) C_L(u,v) S_R(u,v)$.

In our calibration approach, for each image, the data of three surfaces $\aleph_1$, $\aleph_2$ and $\aleph_3$ are acquired simultaneously, keeping the geometrical and reflectance coefficients ($R_{\aleph_1}(\lambda)$, $R_{\aleph 2}(\lambda)$) constant for surfaces $\aleph_1$ and $\aleph_2$ along the calibration procedure. The reflectance of the third surface is varied from image to image. Let

$$\beta(t,t_1) \equiv \frac{Z(\aleph_1,\aleph_2,t)}{Z(\aleph_1,\aleph_2,t_1)} \tag{6}$$

such that $Z(\aleph_1,\aleph_2,t) \equiv \frac{1}{\|\aleph_1\| s(t)} \sum_{(u,v)\in\aleph_1} \sum_{t\in s(t)} \xi(u,v,t) - \frac{1}{\|\aleph_2\| s(t)} \kappa(\aleph_1,\aleph_2) \sum_{(u,v)\in\aleph_2} \sum_{t\in s(t)} \xi(u,v,t)$. $\|\aleph\|$ represents the number of points in $\aleph$ and $s(t)$ is the number of images taken to compute the average image at instant t. It can be shown that $E[\beta(t,t_1)] = A(t)/A(t_1)$, for $\aleph_1$ spatially near $\aleph_2$, and that $V[\beta(t,t_1)] \leq \frac{1}{\|\aleph_2\| s(t)} \left(\frac{1}{Z(\aleph_1,\aleph_2,t_1)}\right)^2 \left(\sigma_N^2(\aleph_1,t) + \kappa(\aleph_1,\aleph_2)^2 \sigma_N^2(\aleph_2,t)\right)$ (E is the expectation operator and V is the variance operator; it is considered that $\|\aleph_1\| = \|\aleph_2\|$ and that $s(t_1)$ is chosen large enough so that the variance of $\beta(t,t_1)$ is mainly conditioned by the noise at instant t). Hence, to have low estimation variance one should have large values for (i) $\|\aleph_i\|$, $i = 1,2$, (ii) $s(t)$ and (iii) $Z(\aleph_1,\aleph_2,t_1)$ (this can be achieved by choosing a white and a black reference surfaces for $\aleph_1$ and $\aleph_2$. $\kappa(\aleph_1,\aleph_2)$ can be computed from dark images, for instance by taking an image with the lens cap on. If a sequence of s images with $I(\lambda,u,v) \equiv 0$ are averaged, then $\xi(u,v,t) = A(t)\{K_D(u,v)\eta(\tau(t)) + N_o(u,v)\} + N(u,v,t)$ (note that if automatic gain is turned off and a large value for s is used, then, due to the independence of A and the noise sources, $A(t) \approx E(A)$) and the signal's variance decreases linearly with s, since $V[\xi(u,v,t)] = \frac{\sigma_N^2}{s}$. From this averaged image it is possible to compute $\kappa(\aleph_i,\aleph_j)$, with the required accuracy by fixing s. Let $\kappa(\aleph_i,\aleph_j)$ be defined by (7) and let $\xi(u,v,t_0)$ be a reference dark image. From (7) it is seen that if s is taken large enough then the expected value can be approximated by (8). In practice, $\kappa(\aleph_i,\aleph_j)$ should be obtained from distinct dark images using robust averaging. Let $\overline{\kappa}(\aleph_i,\aleph_j)$ and σ_κ^2 be the mean and the variance of the set of computed $\kappa_w(\aleph_i,\aleph_j)$ from different dark images and let w_1 be a subset such that $w_1 = \{w : |\kappa_w(\aleph_i,\aleph_j) - \overline{\kappa}(\aleph_i,\aleph_j)| \leq p\sigma_\kappa\}$. If the estimator is defined by $\kappa(\aleph_i,\aleph_j) = \|w_1\|^{-1} \sum_{w\in w_1} \kappa_w(\aleph_i,\aleph_j)$, it is observed that the variance of the estimate is less than $p^2 \sigma_\kappa^2 / \|w_1\|$.

$$\kappa(\aleph_i,\aleph_j) \equiv \frac{\frac{1}{\|\aleph_j\|} \sum_{(u,v)\in\aleph_j} \xi(u,v,t) - \xi(u,v,t_0)}{\frac{1}{\|\aleph_i\|} \sum_{(u,v)\in\aleph_i} \xi(u,v,t) - \xi(u,v,t_0)} \tag{7}$$

$$E[\kappa(\aleph_i,\aleph_j)] \to \frac{\frac{1}{\|\aleph_j\|} \sum_{(u,v)\in\aleph_j} K_D(u,v)}{\frac{1}{\|\aleph_i\|} \sum_{(u,v)\in\aleph_i} K_D(u,v)} \tag{8}$$

The change in additive error can be computed and eliminated as follows: let $\Delta(\aleph_i,t,t_1)$ be defined by

$$\Delta(\aleph_i,t,t_1) \equiv \frac{\sum_{(u,v)\in\aleph_i} [\xi(u,v,t) - \beta(t,t_1)\xi(u,v,t_1)]}{\|\aleph_i\|} \tag{9}$$

The expected value of Δ is given by (10) for $(u,v) \in \aleph_3$ and by (11) for $(u,v) \in \aleph_i$, $i = 1,2$. Therefore, an image without bias can be obtained from (12).

$$E(\Delta(\aleph_i,t,t_1)) = A(t) \frac{1}{\|\aleph_i\|} \sum_{(u,v)\in\aleph_i} C(u,v) \times \int_{\lambda_0}^{\lambda_n} Q(\lambda)[R(\lambda,t) - R(\lambda,t_1)]\,d\lambda + D(\aleph_i,t,t_1) \tag{10}$$

$$E(\Delta(\aleph_i,t,t_1)) = D(\aleph_i,t,t_1) \tag{11}$$

$$D(\aleph_i,t,t_1) \equiv \frac{A(t)[\eta(t) - \eta(t_1)]}{\|\aleph_i\|} \sum_{(u,v)\in\aleph_i} K_D(u,v)$$

$$\zeta(\aleph_3,t,t_1) \equiv \Delta(\aleph_3,t,t_1) - \kappa(\aleph_i,\aleph_3)\Delta(\aleph_i,t,t_1) \tag{12}$$

Combining (10), (11) and (12) and writing the integrals in matrix format using trapezoidal integration with step size $\Delta\lambda$, it follows

$$U(t)Q = 0 \tag{13}$$

$$U(t) \equiv [\alpha(\aleph_3,t) R(t_2) - (1 - \alpha(\aleph_3,t)) R(t_1) - R(t)]^T$$

$$\alpha(\aleph_3,t) \equiv \frac{\beta(t_2,t)\zeta(\aleph_3,t,t_1)}{\zeta(\aleph_3,t_1,t_2)} \tag{14}$$

and $R(t_i) = [R(\lambda_0,t_i), R(\lambda_0+\Delta\lambda,t_i), ..., R(\lambda_n,t_i)]^T$, $Q = [Q(\lambda_0), Q(\lambda_0+\Delta\lambda), ..., Q(\lambda_n)]^T$.

3. Spectral calibration of light sensors

Equation (13) enables the computation of Q if the reflectance $R(t)$, $t = t_1, ..., t_{m+2}$, of reference surfaces are known. Namely, if $m+2$ images are taken such that $R(t_i) \neq R(t_j)$, $i \neq j$, then $A\overline{Q} = B$, $B^T = \begin{bmatrix} 0 & K \end{bmatrix} \in \mathbb{R}^{l\times n}$, $A^T = \begin{bmatrix} U^T(t_3) & ... & U^T(t_{m+2}) & \Delta\lambda I_V \end{bmatrix} \in \mathbb{R}^{n\times m}$ and $I_V^T = \begin{bmatrix} 1 & \cdots & 1 \end{bmatrix} \in \mathbb{R}^{1\times n}$. The normalization introduced in $\overline{Q}$ ($Q \equiv K\overline{Q}$) is performed to avoid the trivial solution of (13). If the same normalization gain K is to be

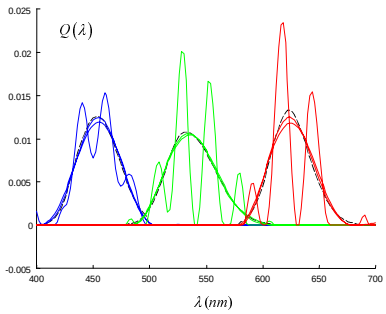

Figure 1. Continuous curves - estimated curves for $\sqrt{\gamma} = 0.01, 1, 5$, dotted curves - ideal values.

applied for each of the camera's channels then the procedure we have described in [2] may be used to compute K. However, for most applications K can be chosen such that $K \in \mathbb{R}^{+}$.

Formulating the spectral calibration problem in terms of a quadratic criterion minimization subject to linear constraints, it is seen that the criterion is described by (15) (the regularization term based on the discrete approximation $\frac{D}{\Delta\lambda^2} \in \mathbb{R}^{(n-2)\times n}$ of the second derivative of $\overline{Q}$ is imposed for smoothness purposes) subject to positivity, that is, $\overline{Q}_i \geq 0, i = 1, \cdots, n$. This is an intrinsic physical constraint, since light sensor cells do not emit light.

$$E = \frac{\Delta\lambda}{m\sigma^2}\left\|A\overline{Q} - B\right\|^2 + \frac{\alpha}{\Delta\lambda^4}\left\|D\overline{Q}\right\|^2, \alpha \in \mathbb{R}^{+} \quad (15)$$

From figure 1 it can be observed that for small values of α the estimation of $\overline{Q}\,(\lambda)$ exhibits oscillations. As α increases, these oscillations are attenuated due to the added importance of the second derivative term. However, for large α it is observed that the solution tends to smooth excessively local maxima. In [3] we have used this observation to derive additional constraints to improve the solution of (15). However, the method exhibits two unsolved problems, namely: (i) which is the best $\gamma \equiv \frac{m\alpha\sigma^2}{\Delta\lambda^5}$ for the problem and (ii) the maxima estimation technique can produce relatively large estimation errors whenever $Q\,(\lambda)$ is band-limited and the channel is tuned for a spectral region where $R\,(\lambda, t_i)$ are almost linearly dependant. For instance, from fig. 4 it is observed that for the red channel the simple estimation technique enables lower SSE (Sum Squared Error) values than the maxima constraining technique, although the later exhibits a much smoother SSE evolution curve. This is mainly due to the maxima extrapolation error.

3.1. The GCV_{IC} measure

Equation (15) corresponds to the estimation of a spline in the general sense [7]. Hence, we might test how well the estimated spline predicts the data for different roughness penalty values γ. This idea was first applied by Wahba [7] and resulted in the introduction of the GCV (generalized cross-validation) measure for the unconstrained fitting problem. In this work, the GCV is extended to the linear inequality constrained fitting problem. This extension results in a new GCV measure, the GCV_{IC}.

Let $(\lambda_M, \widehat{Q}_M)$ be the estimated maxima. The fitting problem may now be written as

$$\min\{E\} : E = \left\|A^*(\gamma)\,\overline{Q} - B^*\right\|^2 \quad (16)$$

$$\text{subject to } C(\lambda_M)\overline{Q} \leq H(\widehat{Q}_M) \quad (17)$$

$$A^*(\gamma) = \begin{bmatrix} A \\ \sqrt{\gamma}D \end{bmatrix}, B^* = \begin{bmatrix} B \\ 0 \end{bmatrix} \quad (18)$$

where C and H are formed to describe the following constraints: (i) $\overline{Q}_i \geq 0, i = 1, \ldots, M-2, M+2, \ldots, n$, (ii) $\overline{Q}_M = \widehat{Q}_M$, (iii) $\overline{Q}_{M-1} \leq \overline{Q}_M$ and $\overline{Q}_{M+1} \leq \overline{Q}_M$. From the active set theory [6] it is known that the solution to the problem in (16) and (17) is equivalent to solve an equality constrained problem with the subset of constraints which, for a particular solution, are active, i.e., are verified with equality. Let $C^* \subseteq C(\lambda_M)$ and $H^* \subseteq H(\widehat{Q}_M)$ be the subset of constraints in (17) verified with equality, then the solution can be found using the following theorem:

Theorem 1 *The best approximate solution to the equality constrained problem in (19) is (20). (for proof see [6])*

$$\min_x \|AX - B\|^2 \text{ subject to } C^*X = H^* \quad (19)$$

$$X = \sum_{i=1}^{p}\left(\widetilde{d}_i/\beta_i\right)z_i^* + \sum_{i=p+1}^{n}\widetilde{b}_i z_i^* \quad (20)$$

where $A = W_A\begin{bmatrix} D_A^T & 0 \end{bmatrix}^T Z$, $C^* = W_C\begin{bmatrix} D_C & 0 \end{bmatrix}Z$ *are the generalized singular value decompositions of* A *and* B, $\widetilde{b} = W_A^T B$, $\widetilde{d} = W_C^T H^*$, $Z^{-1} = \begin{bmatrix} z_1^* & \cdots & z_n^* \end{bmatrix}$, $D_A = diag(\alpha_1, \ldots, \alpha_n)$ *and* $D_C = diag(\beta_1, \ldots, \beta_p)$.

Corollary 2 *Let* $\widehat{Q}(\gamma, \lambda_M, \widehat{Q}_M)$ *be the solution to (16) and (17) using the active set theory. Then, if* $C^*\widehat{Q} = H^*$ *are the subset of active constraints,* $\widehat{Q}$ *verifies*

$$\widehat{Q}(\gamma, \lambda_M, \widehat{Q}_M) = \Omega(\gamma, \lambda_M, \widehat{Q}_M) + \Theta(\gamma, \lambda_M, \widehat{Q}_M)B \quad (21)$$

with $\Omega(\gamma,\lambda_M,\widehat{Q}_M)=Z_1D_C^{-1}W_C^TH^*$, $\Theta(\gamma,\lambda_M,\widehat{Q}_M)=Z_2W_{21}$, $Z^{-1}=\begin{bmatrix}\underbrace{Z_1}_{p} & \underbrace{Z_2}_{p-k}\end{bmatrix}$, *Z, W_C, DC, W_A defined as in theorem 1, and*

$$W_A^T=\begin{bmatrix}\overbrace{W_{11}}^{m} & \overbrace{W_{12}}^{n-2}\\ W_{21} & W_{22}\\ W_{31} & W_{32}\end{bmatrix}\begin{matrix}p\\ n-p\\ m-2\end{matrix}$$

Proof is immediate by taking theorem 1 and the formulation in (16) and several simple algebraic manipulations.

The above corollary is the framework to derive the GCV_{IC} measure, which is based on the definition of the ordinary cross-validation function [7]. Let $\widehat{Q}^{[k]}(\gamma,\lambda_M,\widehat{Q}_M)$ denote the spline estimate of $\overline{Q}$ using all but the kth data point of B. The OCV function measures the overall predictability of data points by the estimate $\widehat{Q}(\gamma,\lambda_M,\widehat{Q}_M)$ and is defined by (B_k - kth element of vector B; A_k - kth row vector of matrix A)

$$OCV_{IC}=\frac{1}{m}\sum_{k=1}^{m}(B_k-A_k\widehat{Q}^{[k]}(\gamma,\lambda_M,\widehat{Q}_M))^2 \qquad (22)$$

To derive the GCV_{IC} function from (22) some theorems have to be introduced. For notation simplicity, let $X^{[k]}\equiv\widehat{Q}^{[k]}(\gamma,\lambda_M,\widehat{Q}_M)$, then:

Lemma 3 *(extension of lemma 3.1 of Craven and Wahba) Let $h(k,z)$ be the solution to (16) with linear equality constraints and with the kth data point replaced by z, then $h(k,A_kX^{[k]})=X^{[k]}$.*

Proof. From the definition of $X^{[k]}$ it is seen that the solution is obtained from (the constraints are omitted for simplicity)

$$\min\left\|\begin{bmatrix}I&0&0\\0&0&I\end{bmatrix}^T\left(A^*(\gamma)X^{[k]}-B^*\right)\right\|^2\iff$$

$$\min\left\|\begin{bmatrix}I&0&0\\0&0&I\end{bmatrix}^T\left(A^*(\gamma)X^{[k]}-B^*\right)+\begin{bmatrix}0&A_k^T&0\end{bmatrix}^T\left(X^{[k]}-X^{[k]}\right)\right\|^2 \qquad (23)$$

Equation (23) can equivalently be written by

$$\min\left\|A^*(\gamma)X^{[k]}-\widetilde{B}\right\|^2$$

with $\widetilde{B}^T=\begin{bmatrix}B_1&\cdots&A_kX^{[k]}&\cdots&B_m&0\end{bmatrix}$, which corresponds to the definition of $h(k,A_kX^{[k]})$. ■

Theorem 4 *The OCV_{IC} function for the problem defined in (16) with linear equality constraints is*

$$OCV_{IC}=\frac{1}{m}\sum_{k=1}^{m}\frac{(B_k-A_kX)^2}{(1-\rho_{kk})^2} \qquad (24)$$

where ρ_{kk} is the kkth element of $A\Theta(\gamma,\lambda_M,\widehat{Q}_M)$ and $\Theta(\gamma,\lambda_M,\widehat{Q}_M)$ is as defined in (21) and $X\equiv\widehat{Q}(\gamma,\lambda_M,\widehat{Q}_M)$.

Proof. To proof this theorem we will show that

$$B_k-A_kX=(1-\rho_{kk})\left(B_k-A_kX^{[k]}\right)$$

Let Ω_k^1 be the kth element of $A\Omega$. From the lemma 3, the above equation is equivalent to $(1-\rho_{kk})(B_k-A_kh(k,A_kX^{[k]}))=B_k-A_kX$. Let $B_k^*\equiv A_kh(k,A_kX^{[k]})$. From the definition of h and using (21) it is seen that

$$B_k^*=\Omega_k^1+\rho_k\begin{bmatrix}B_1&\cdots&B_k^*&\cdots&B_m\end{bmatrix}^T\iff$$
$$(1-\rho_{kk})(B_k-B_k^*)=$$
$$(1-\rho_{kk})B_k-\rho_k\begin{bmatrix}I&0&0\\0&0&I\end{bmatrix}^TB-\Omega_k^1=$$
$$\begin{bmatrix}-\rho_{k1}&\cdots&1-\rho_{kk}&\cdots&\rho_{km}\end{bmatrix}B-\Omega_k^1$$

On the other hand, $B_k-A_kX=\begin{bmatrix}0&1&0\end{bmatrix}B-\rho_kB-\Omega_k^1=\begin{bmatrix}-\rho_{k1}&\cdots&1-\rho_{kk}&\cdots&\rho_{km}\end{bmatrix}B-\Omega_k^1$. ■

Theorem 5 *The GCV_{IC} function for the problem defined in (16) with linear equality constraints is*

$$GCV_{IC}=\frac{\frac{1}{m}\|B-AX\|^2}{\left(\frac{1}{m}trace\,(I-\rho)\right)^2} \qquad (25)$$

Proof. Proof is immediate by taking a weighted OCV_{IC} to account for nonequally spaced data points. It can be shown that ρ is symetric. Hence, following Wahba, it is possible to find a transformation Γ such that $\Gamma A\Gamma^T$ is circulant. Taking the OCV_{IC} on this new system, it is seen that the points are equally spaced and the transformation is equivalent to take the weights $w_k=\left[(1-\rho_{kk})/\frac{1}{m}trace(I-\rho)\right]^2$. ■

3.2. The learning algorithm

Equation (25) can be applied to find the best set of parameters $(\gamma,\lambda_M,\widehat{Q}_M)$ for the estimation problem in (16) and (17). Namely, $\widehat{Q}$ can be computed from (16) and (17), such that (25) is minimized.The GCV_{IC} function is nonlinear and, therefore, a nonlinear optimization technique is required. In this paper we use a genetic algorithm approach, since it is able to perform a parallel exploration of the search space [14] and does not suffer from local minimum problems. Our approach is summarized in figure 2. First a set

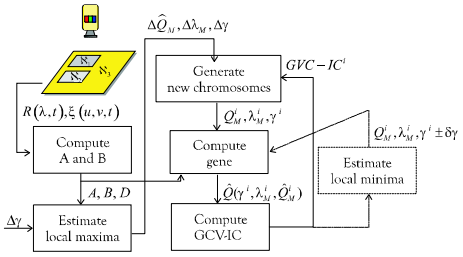

Figure 2. Spectral calibration algorithm.

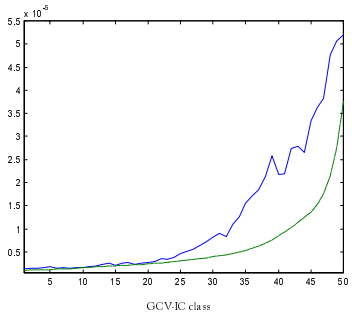

Figure 3. Relation between SSE (continous) and GCV_{IC} (dashed) for red calibration curve in figure 4 (curves scaled to the same scale). These curves were obtained from 5000 chromosomes sorted by their GCV_{IC} and averaged in classes of 100 chromosomes.

of images of surfaces with known spectral reflectance are acquired with the camera whose sensor(s) is to be characterized. These images enable the computation of matrixes A and B. Using the algorithm introduced in [3], the function's maxima are estimated. Let $Q(\lambda_M, \gamma_1)$ be the local maxima obtained with the regularization gain γ_1, such that γ_1 is the lower limit of the identified stable regularization gain interval (gains which do not induce oscillation of the identified function). The search interval for local maxima is defined by $\Delta\widehat{Q}_M = [\max\{0, |\widehat{Q}_M - \delta\widehat{Q}_M - Q(\lambda_M, \gamma_1)|\}, \widehat{Q}_M + \delta|\widehat{Q}_M - Q(\lambda_M, \gamma_1)|]$, $\delta \in [1, \infty[$, where $\widehat{Q}_M$ is the estimated maxima with the algorithm we have introduced in [3]. Parameter δ is not critical, since it simply establishes a search range for the local maxima. In our tests we have fixed $\delta = 2$, however, larger values may be applied. The only reason for not using very large values for δ is that the search space will be enlarged, increasing, therefore, the computational load. To compute $Q(\lambda_M, \gamma_1)$ and $\widehat{Q}_M$ the algorithm requires that a search interval $\Delta\gamma$ of regularization gains to be specified. The lower limit of this interval should be chosen such that the identification result exhibits strong oscillation (in our tests we use 0.01). On the other hand, the upper interval limit should be chosen such that it produces a very smooth estimation (we use 5). The exact interval limits are not critical, since, if a very high upper limit is specified, the algorithm is able to correct it (for details refer to [3]). As for the lower interval limit, it suffices if it induces oscillation of the solution of (15) subject to the positivity constraint. If λ_M is to be searched, then a search interval $\Delta\lambda_M$ should be specified at this stage. In our implementation, λ_M is fixed and equal to λ_M retrieved from the maxima estimation method, for two reasons: (i) it can be shown that if the neighborhood of the local maxima is reasonably symmetrical, then it will be located at the same wavelength(s) for any regularization gains, as long oscillation is avoided, and (ii) another search parameter increases dramatically the computational load.

Once the search space $(\Delta\widehat{Q}_M, \Delta\lambda_M, \Delta\gamma)$ has been established a genetic algorithm is applied to minimize the GCV_{IC} measure. The implemented genetic algorithm uses binary coding, being the size l of each chromossom $(\widehat{Q}_M^i, \lambda_M^i, \gamma^i)$, $i = 1, ..., 1.5l$ ($1.5l$ - the population size), a function of the intended precision for each of its variables. As for the initialization, 50% of the chromosomes are initialized randomly and for the other 50%, $\widehat{Q}_M^i$ is a result of evenly dividing the search space $\Delta\widehat{Q}_M$, with γ^i on the upper limit of $\Delta\gamma$. Selection and sampling are performed with the ranking strategy and the universal stochastic sampling algorithm, respectively [15]. Selection is performed on the GCV_{IC} measure for each of the chromosomes. The chosen genetic operators are the multi-point crossover operator with a crossover probability of 1 and the mutation operator with a mutation probability of $1/l$ (approx. 0.05). Generational reproduction is applied. Given a chromosome $(\widehat{Q}_M^i, \lambda_M^i, \gamma^i)$, two strategies can be applied: (i) the algorithm computes $\widehat{Q}(\widehat{Q}_M^i, \lambda_M^i, \gamma^i)$ with (16) and (17), and, using this result computes the predictability of the solution, i. e., GCV_{IC}^i and returns to the GA for the next iteration, or (ii) the algorithm computes $min_\gamma GCV_{IC}^i$ using $(\widehat{Q}_M^i, \lambda_M^i)$ and γ^i as a starting point (this is represented in figure 2 by the dashed components). The second strategy can be implemented with a line search algorithm or a gradient descendent method. In our implementation we use the golden section search algorithm. From our tests, it seems that this strategy enables faster convergence.

4. Results and conclusions

To objectively measure the performance of the described method, a simulation program was developed as suggested in [4] and using the image formation model introduced in (1). Phong's model was applied to obtain light reflection results. All images were computed with interface and body reflections. The lens was modeled with a pinhole model with focal center and aperture attenuation. Since the main

noise source in image formation is normally distributed [11] with a standard deviation usually in the range $\sigma_N \in [2, 6]$ [1] we modeled the noise to be a linear function of the μ_ξ, such that $\sigma_N = 2$ for $\mu_\xi = 10$ and $\sigma_N = 6$ for $\mu_\xi = 250$. The sensor's dark current noise was assumed to be $\eta(t) = 10 + \delta(t)$ RGB units, with $\delta(t) \in [-2, 2]$ being a random offset. The sensor's channel gain $A(t)$ was considered to vary $A(t) = A_0(t)(1 + \delta_A(t))$, $\delta_A(t) \in [-0.1, 0.1]$, and $A_0(t)$ was computed such that for a white surface the maximum camera output does not clip. As illumination source, the SPD of a Tungsten lamp was applied, with a gain change $G(t) = 1 + \delta_G(t)$, $\delta_G(t) \in [-0.1, 0.1]$. In this paper we present the calibration results obtained with this illumination source combined (i) with a asymmetrical Gaussian model for $S(\lambda)$ (these are typical sensitivity curves for some cameras such as the Sony DXC-930 color video camera [1]) and (ii) with the spectral sensitivity curves from a Kodak DCS200 camera obtained with the algorithm described in [19]. These two types of sensitivity functions were chosen to evaluate the method's performance for curves with distinct smoothness and modality. In these testes 24 patches of the MacBeth-Color Checker map were applied. For each surface, 10 images were taken and averaged. Finally, the sampling step was fixed to $\Delta\lambda = 2nm$ and the SSE (Sum Squared Error) values were computed by $SSE = \left\| Q_{\text{real}} - \widehat{Q}(\widehat{Q}_M, \lambda_M, \gamma) \right\|^2$, where Q_{real} represents the real function. In fig. 3 the relation between SSE and GCV_{IC} evolution is depicted. As can be observed, $GCV_{IC} \uparrow$ when $SSE \uparrow$, being therefore an ideal function for learning the intended parameters, which for other methods have to be arbitrated based on *a priori* knowledge on the spectral curves. The estimation results are exhibited in fig 4 and fig. 5. A summary of the applied conditions and obtained results can be found in table 1. Fitting without maxima constraints exhibit rapid varying SSE values with γ. Constraining maxima enables much better estimation results, since slower varying and lower SSE values are feasible in this case. However, whenever $\widehat{Q}_M$ is not identified in the vicinity of the real maxima, it is seen that the approximation errors tend to be much higher as compared to the best SSE values obtained without maxima constraints. Further, for both methods, in real situations, it is not possible to know where the SSE minima is located. These disadvantages are solved with the GCV_{IC} based method, which enables the automatic selection of the "best" set of constraints and regularization gain. For instance, for the red channel's curve in fig. 4, the GCV_{IC} based method obtains an approximation whose SSE is more than 300% lower than the best SSE obtained with the simple identification method and more that 500% lower than the best SSE computed with the maxima constraints based algorithm. This is possible, because neither of the former methods ever come near to correctly estimate the maxima. It is observed that the

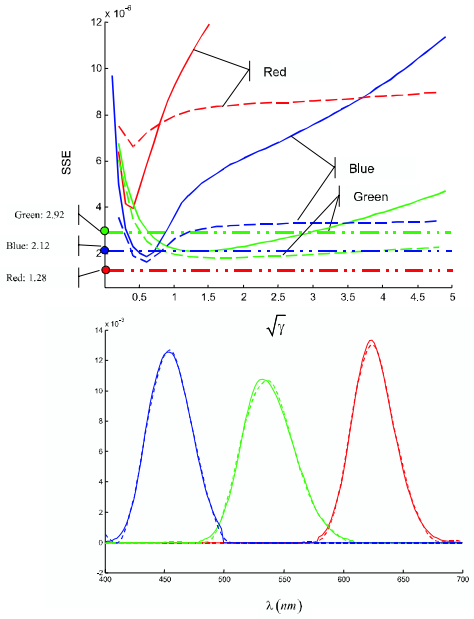

Figure 4. Assymmetrical Gaussians. Top: SSE evolution with γ. Continuous curves SSE of the solution without maxima constraints; dashed curves - SSE of the solution with maxima constraints; dash-point curves - best estimate with GCV_{IC} (γ not shown). Bottom: $\overline{Q}$ - continuous curves; $\widehat{Q}$−dashed curves.

GCV_{IC} based method enables the identification of suboptimal solutions in the vicinity of the global minimum. This behavior is in accordance with Wahba's theorem 4.2 [7], since the global optimum is not attainable, since the "expectation efficiency" is usually less than 1.

This paper introduces a new fitting technique for the illposed sensor's spectral calibration problem. In our method, based on a new GCV_{IC} measure, no *a priori* knowledge on the sensor's characteristics is required, since the method is able to learn the needed constraints and the regularization gain from the input data. This is a relevant result because knowledge on the sensor's spectral characteristics is in most cases very difficult or even impossible to obtain with the required accuracy. Further, these characteristics may vary significantly as sensors age [5] (for instance through color filter transmittance changes with aging). We have also introduced a physics-based image formation model that accounts for multiplicative and additive error changes with time. Using this model we have shown how to compensate for changing error sources. Finally, the outlined strategies can be easily adapted to similar problems, as for example, for spectral reflectance estimation.

Acknoledgements: This project was partially financed

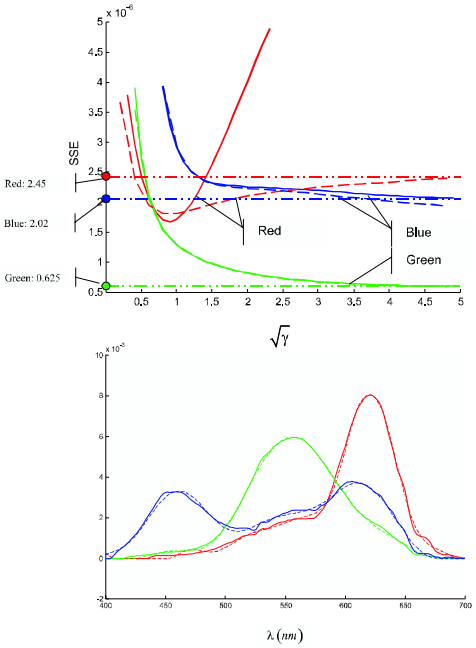

Figure 5. KodakDCS200. Top: SSE evolution with γ. Continuous curves SSE of the solution without maxima constraints; dashed curves - SSE of the solution with maxima constraints; dash-point curves - best estimate with GCV_{IC} (γ not shown). Bottom: $\overline{Q}$ - continuous curves; $\widehat{Q}$−dashed curves.

by FCT/PRAXIS XXI (project 36564/99), and POSI (Programa Operacional Sociedade de Informação of the Portuguese Government supported by the European Union), and was performed at the Computational Perception Laboratory at CISUC.

References

[1] K. Barnard and B. Funt. Camera calibration for color research. In *Proc. SPIE Electronic Imaging IV*, 1999.

[2] P. Carvalho, A. Dourado, and B. Ribeiro. CCD sensor spectral sensitivities estimation without a spectroradiometer. In *11th Portuguese Conf. On Pattern Recognition*, pages 205–212, 2000.

[3] P. Carvalho, A. Dourado, and B. Ribeiro. Improving error stability in spectral camera calibration for color inspection with maxima constraints. In *6th Int. Conf. On Control, Automation, Robotics and Vision*, 2000.

[4] P. B. Catrysse, B. Wandell, and A. E. Gamal. Comparative analysis of color architectures for image sensors. In *SPIE*, 1999.

[5] Y.-C. Chang and J. F. Reid. RGB calibration for color image analysis in machine vision. *IEEE Trans. on Image Processing*, 5(19):1414–1422, 1996.

$Curve$	$\Delta\widehat{Q}_M$	$\overline{Q}_M$	$\widehat{Q}_M$	SSE
GR	[0.0102,0.0139]	0.0133	0.0131	1.28E-6
GG	[0.0102,0.0108]	0.0107	0.0107	2.92E-6
GB	[0.0114,0.0128]	0.0126	0.0127	2.21E-6
KR	[0.00643,0.00881]	0.00804	0.00815	2.45E-6
KG	[0.00594,0.00598]	0.00594	0.00598	6.25E-7
KB	[0.00360,0.00374]	0.00377	0.00373	2.02E-6

Table 1. Simultaion results. GX - Gaussian curves; KX - Kodak DCS200; X (R-red, G-green, B-blue)

[6] P. Ciarlet and J. Lions. *Handbook of Numerical Analysis*. Elsevier-North Holland, 1990.

[7] P. Craven and G. Wahba. Smoothing noisy data with spline functions. *Numer. Math.*, 31:377–403, 1979.

[8] J. Farrell, J. Cupitt, D. Saunders, and B. Wandell. Estimating spectral reflectances of digital artwork. In *Chiba Confernce on Multispectral Imaging*, 1999.

[9] G. Finlayson and S. Hordley. Recovering device sensitivity with quadratic programming. In *IST/SID's Color Imaging Conf.: Color Science, Systems and Applications*, pages 90–95, 1998.

[10] H. Haussbecker. Radiometry of imaging. In B. Jähne, H. Haussbecker, and P. Geissler, editors, *Handbook of Computer Vision and Applications*, pages 103–136. Academic Press, 1999.

[11] G. E. Healey and R. Kondepudy. Radiometric CCD camera calibration and noise estimation. *IEEE Trans. on Pattern Anal. Machine Intell.*, 16(3):267–276, 1994.

[12] P. Hubel, D. Sherman, and J. Farrell. A comparison of methods of sensor spectral sensitivity estimation. In *IST/SID's Color Imaging Conf.: Color Science, Systems and Applications*, pages 45–49, 1994.

[13] R. Lee. Colorimetric calibration of digitizing systems: Algorithm and application. *Color Research and Application*, 13(3):180–186, 1988.

[14] Z. Michalewicz. *Genetic Algorithms+Data Structures=Evolution Programs, Third Revised and Extended Edition*. Springer Verlag, 1996.

[15] A. Santos and A. Dourado. Global optimization of energy and production in process industries: A genetic algorithm application. *Control Engineering Practice*, 7(4):549–554, 1999.

[16] P. Seitz. Solid-state image sensing. In B. Jähne, H. Haussbecker, and P. Geissler, editors, *Handbook of Computer Vision and Applications*, chapter 7, pages 165–222. Academic Press, 1999.

[17] G. Sharma and H. Trussel. Characterization of scanner sensitivity. In *Color Imaging Conf.: Transformations and Transportability of Color*, pages 103–107, 1993.

[18] L. A. Spoomer and M. A. L. Smith. Image analysis for biological research: Camera influence on measurement accuracy. *Intell. Instrum. Comput.*, pages 201–215, 1988.

[19] P. Vora, J. Farrell, J. Tietz, and D. Brainard. Digital color cameras - 2 - spectral response. Technical Report HPL-97-53, Hewlett-Packard Lab., 1997.